Korean J. Chem. Eng., 38(12), 2479-2492 (2021)
DOI: 10.1007/s11814-021-0973-3

pISSN: 0256-1115
eISSN: 1975-7220

Preparation of eco-friendly wax-coated paper and its rheological and water-resistant characteristics

Eun Ju Lee and Kwang-Hee Lim†

Dept. of Chem. Eng., College of Engineering, Daegu University, Gyeongsan, Gyeongbuk 38453, Korea
(*Received 28 May 2021 • Revised 10 September 2021 • Accepted 1 October 2021*)

Abstract−The blend (wax M) of crude by-product polyolefin wax (wax K) and a fractionated commercial paraffin wax (wax J) was suggested to replace the wax J as a coating agent for wax-coated papers. The rheological properties of waxes J, K, and M were examined and compared. The correlation between viscosity and shear rate applied on these waxes maintained at 90 °C and 130 °C was identified. In particular, this paper, for the first time, presented non-Newtonian shear thinning behavior of not only wax K but also its blend of wax M in terms of their viscosity affected by shear rate at an operating temperature below their melting temperature of higher-melting-temperature DSC endothermic peaks (HMTEPs). They showed non-Newtonian behavior, so-called shear thinning behavior, at 90 °C in the light of characteristics of both suspension systems and polymer systems. In addition, the profiles of viscosity at 130 °C of all the waxes versus the shear rate exhibited Newtonian fluid behavior. Wax J also showed the behavior of a dilatant fluid. Then, the physical properties including water vapor transmission rates (WVTR), surface roughness, and coated weights, of thin papers coated with waxes J (WJP), K (WKP), and M (WMP) were evaluated, characterized, and compared. As a result, WMP had an equivalent value to that of WJP or the lowest value among wax-coated papers in terms of WVTR. The surface roughness and the barrier property of WVTR were minimized and enhanced, respectively, by blending waxes J and K. The additional physical properties, including dynamic contact angles, surface tension, wet and dry tensile strength, optical examination of the wax-coated fiber structure, and antimicrobial properties of the wax-coated papers, were evaluated. The excellent antimicrobial properties of clinoptilolite added to wax J or wax M appeared.

Keywords: Crude Byproduct Polyolefin Wax, Paraffin Wax, Blend, Wax-coated Papers, Viscosity, Water-resistance, Barrier Property, Surface Roughness, Antimicrobial Property

INTRODUCTION

Byproduct wax is generated mainly on a large scale as a byproduct from facilities producing commercial polyethylene or polypropylene. Most such wax is being disposed of by the regulations from the ministry of environment on treating waste materials. Therefore, it is necessary to recycle the byproduct wax, which may replace expensive commercial paraffin wax. In general, polymers, such as polyethylene or polypropylene, have been used as fruit packaging materials. Although it was reported that polyethylene could be degraded significantly by the microorganisms from Indian meal moths [1,2], they are still barely degradable by environmental microbes. Hence, they are not considered environmentally friendly materials, such as paper. On the other hand, polyethylene wax was reported to become a faster biodegradable material by a bacterial consortium of KH-12 and a fungus of Aspergillus sp. as its molecular weight becomes lower [3]. Thus, wax-coated paper may satisfy the requirements of water resistance and environmental friendliness from the superior biodegradability of low molecular weighted wax-coated paper compared to high molecular weighted polymers.

Several studies have examined the characterization of various waxes or various waxes coated on substrates. Bucio et al. [4] characterized paraffin wax, beeswax, and candelilla wax for coating cheese. They reported that the water vapor transmission rate (WVTR) of paraffin wax was equivalent or lower than that of beeswax but was only 23% of candelilla wax. Mishra et al. [5] investigated the viscosity, WVTR, and O_2/CO_2 permeability of edible coatings, including beeswax. Once temperatures reach the melting point of paraffin wax, which can vary between 40 °C and 80 °C with wax type, it becomes a liquid with Newtonian properties [6,7]. Czarneck-Komorowska et al. [8] examined the influence of bentonite on the rheological properties, linear shrinkage, hardness, and structure of polyethylene wax used in the lost-wax casting process. In their study on the viscosity of polyethylene wax, the viscosity of the wax, having a melting temperature of 60 °C, filled with various amounts of bentonites, was determined using a rotational rheometer at 71 °C. Even though unmodified polyethylene wax, similarly to compositions containing very low concentration (e.g., 0.1 and 0.4 wt%) of bentonite, showed no influence of shear rate on viscosity, the phenomenon of shear-thinning behavior and a significant increase in viscosity of filled wax at a low shear rate was observed. They suggested that the significantly higher viscosity values at low shear rates were likely the result of the occurrence of agglomerated filler structures. Similarly, Liu et al. [9] reported that nanofluid made by suspending multi-walled carbon nanotubes (MWCNTs) in liquid paraffin should be characterized as a fluid with non-Newtonian behavior of shear-thinning. It was observed that with increasing volume fractions of MWCNTs, the fluid behavior deviates more from Newtonian behav-

†To whom correspondence should be addressed.
E-mail: khlim@daegu.ac.kr

ior decreasing power law index.

Dwivedi et al. [10] examined ten different waxes, including paraffin wax and microcrystalline waxes, using differential scanning calorimetry (DSC) and conventional testing methods. They suggested that the highest thermal transition is a solid-liquid transition associated with complete melting, which can guide the choice of wax storage and application temperatures. Ciesinska et al. [11] investigated the selected thermal properties of polyethylene waxes, which were byproducts formed in the ethylene polymerization process. They reported that the fractionation of waxes caused an increase in their crystallinity. Lee et al. [12] compared the thermal properties of a crude byproduct polyolefin wax (wax K), technical grade-commercial fractionated paraffin wax (wax J), and their blend (wax M). They reported two melting points (i.e., lower/higher melting temperatures) of waxes J, K, and M to be 47.53/64.10 °C, 73.16/116.88 °C, and 59.03/115.18 °C, respectively. Main melting temperatures of waxes J, K, and M corresponded to the latter, the former and the former between the lower/higher melting temperatures reported by Lee et al. [12], respectively. Wax M showed co-crystallization for its sharper lower-melting-temperature DSC endothermic peak (LMTEP), indicating a narrower molecular weight distribution than that of wax K at the melting temperature of 59.03 °C that was even below the main melting temperature of wax J. However, wax M, a blend of wax K and wax J, still had the thermal properties of a higher-melting-temperature DSC endothermic peak (HMTEP) at the melting temperature of 115.18 °C, which were even narrower and lower than those of wax K, respectively. Lee et al. [13] investigated the changes in surface hydrophobicity of wax J, wax K and wax M by deriving a practical criterion to estimate the diffusivity for their surface enrichment of hydrophilic functional groups. The surface properties of wax J and wax M were more hydrophobic than wax K under a water-submerged condition of less than 1 week, despite the similar structure and functional groups on the surfaces of all three waxes under ambient atmospheric conditions.

Katiyara et al. [14] investigated the effect of varying proportions of waxes, namely paraffin wax, bees wax, montan wax, carnauba wax and ceresin wax, in wax mix on surface roughness optimized by Taguchi method. They reported that paraffin wax formed the major contribution towards the surface roughness, which was varied to be 483 nm, 416 nm and 574 nm according to three levels of used paraffin wax, respectively. Garai et al. [15] studied the effect of raw material composition on water-repellent capacity of paraffin wax emulsions on wood. They reported that two effects were found relating to the distribution of hydrocarbons in paraffin wax affecting its surface properties, such as the contact angle and the surface tension: paraffin wax's intrinsic waterproofing capacity dependent on the hydrocarbons' stereochemical configuration, and the loss of this capacity dependent on the hydrocarbons' molecular weight. Salih et al. [16] analyzed the surface tension and contact angle of paraffin wax using eight types of probe liquids including distilled water, acetone, isopropyl alcohol, methyl methacrylate, dimethyl sulfoxide, ethylene glycol, glycerol and paraffin oil, and water flow simulation for microfluidic device. Based on the contact angle measurements, the hydrophobicity and surface tension of paraffin wax were studied. According to their analysis, for probe liquid of distilled water, the values of surface tension and contact angle were 72.8 mN/m and 90°, respectively. Schuman et al. [17] coated paper board with aqueous dispersions of styrene-butadiene copolymers to improve its surface characteristics. The addition of paraffin wax to the latex dispersion improved the barrier properties of water repellence by decreasing the surface energy, which resulted in an increase in the contact angle of a water drop by a factor of two. The melting point and viscosity at 23 °C of the used paraffin wax were 52 °C and less than 60 mPa s, respectively. Schuman et al. [18] examined the characteristics of polymer coatings on paperboard filled with pigments, such as talc or kaolin clay and paraffin wax, to increase the barrier property of water repellence. The effects of three different commercial waxes (i.e., two paraffin waxes and one paraffin/polyethylene wax) coated on paperboard on water resistance were investigated in terms of the contact angle of a water drop and its surface energy [19]. Cellulose is a hydrophilic (due to a large number of surface hydroxyl groups) and hygroscopic material [20-23]. Despite the basic rough surface morphology, achieving super-hydrophobicity on cellulose materials (e.g., paper) by only hydrophobization treatments (even with fluorine coatings) is very difficult [24-26].

This paper presented the novel feature of blending of wax K and wax J on the rheological properties and the physical and functional properties of the wax-coated papers, where a blend of wax M is suggested to replace wax J. In addition to an analysis of their thermal and functional group-related structural properties as well as their surface hydrophobicity alteration properties by Lee et al. [12] and Lee et al. [13], respectively, the rheological properties of each wax were characterized and compared. In particular, this paper, for the first time, presented the novel rheological behavior of not only wax K but also its blend of wax M in terms of their viscosity affected by shear rates at an operating temperature below their melting temperatures of HMTEPs.

The physical and functional characteristics of each thin paper coated with waxes J (WJP), K (WKP), and M (WMP) were evaluated in terms of the water vapor transmission rate, surface roughness, and coating weight. In this study, wax M, which has similar properties to wax J, was suggested to replace wax J as a coating agent on thin paper. Under the circumstances, the water resistance, wet and dry tensile strength, optical microscopy images of the wax-coated fiber structure, and bacterial resistance of WJP and WMP were examined under various physical and chemical coating conditions of a forward roll coater. The properties of the waxes were compared to construct the optimal coating conditions on a thin paper with wax M to determine if WMP had equivalent characteristics to those of WJP and more feasible operational adaptability.

MATERIALS AND METHODS

1. Materials

Technical grade paraffin wax (wax J) was purchased from Nippon Seiro Co. A crude byproduct polyolefin wax (wax K) was obtained from a naphtha-cracking unit located at the Yeochun-Chemical Complex in Korea. Both wax K and wax J were mixed with a seven to three mass ratio at ambient conditions. The blend was prepared by melt mixing in a Brabender Platograph at 140 °C and a rotation speed of 30 rev./min for 10 min, after which it was

Table 1. Chemical composition of clinoptilolite purchased from Wangpyo company

Component	SiO_2	Al_2O_3	MgO	CaO	Na_2O	Fe_2O_3	LOI
Content (%)	71.0	10.0	1.5	2.2	3.0	2.5	7.0

cooled slowly to room temperature to prepare wax M. The blend, wax M, was kept at room temperature for at least 24 h before the experiments. The wax-coated white thin papers (wax-coated papers) were conditioned under a controlled relative humidity of 50-55% by placing them over a saturated magnesium nitrate solution (500% w/v) at 23±2 °C for three days before their respective analyses and tests [27]. The standard fungus, *Aspergillus Terreus*, was obtained from KCTC. Natural zeolite, clinoptilolite, was purchased from Wangpyo company. Table 1 lists the chemical composition of purchased clinoptilolite.

2. Operating Conditions to Prepare Wax-coated Papers

The two-roll forward roll coater was manufactured with a maximum operating temperature of 200 °C of a heating bath and two rollers (Φ=140 mm), and a maximum operating roller speed of 300 rpm. The two-roll forward roll coater was fed by dip coating from a pan, after which the coating was metered by its passage through a narrow gap between the applicator and backup rolls. The characteristics of thin white papers (thin papers) coated with wax J, wax M, and, if necessary, wax K, were observed at various operating conditions of the coating roll miller. For wax M, the mixing mass ratio of wax K and wax J was seven to three. The operating temperature of the heating bath and two rollers was continued at 120 °C except when N-propanol was tested as a coupling agent. The clearances of the roll millers were set to 30 μm and 70 μm for experiments I and II, respectively. For both experiments I and II, coating characteristics were investigated at three roller speeds of 100 rpm, 150 rpm, and 200 rpm. Under a 90 °C operating temperature of the heating bath and two rollers, N-propanol was tested as the coupling agent between the coated wax and paper to improve the fluidity of the coating wax. Forward roll coating, sometimes referred to as meniscus roll coating, is used most commonly to apply thin optical-quality coatings of low viscosity liquids. Typical operating parameters are 3-60 m/min speed, 1-50 mPa s viscosity liquids, and 25-60 μm wet thickness. In forward roll coating, the coating thickness is sensitive to the speed, viscosity, and gap [28]. Thus, the operating conditions to prepare wax-coated papers may be regarded within the range of the typical operating parameters of forward roll coating. For the test of the antibacterial properties, wax-coated papers were prepared in experiment I at a roller speed of 100 rpm.

3. Rheological Properties of Waxes and Characteristics of Wax-coated Papers

3-1. Viscosity of the Waxes

The viscosities of the melt waxes were measured three times (n=3) per experimental condition using a Brookfield viscometer (Brookfield, RVDVII+) equipped with spindle #3 at 90 °C and 130 °C. The angular speed of the spindle was controlled at five different speeds of 20, 30, 50, 60, and 100 rpm to identify the correlation between the viscosity and shear rates. The viscosity versus shear rate profiles of those waxes were measured using a Physica Rheometer (Anton Paar Instrument, MCR 301) with a guaranteed error range of ±2% for measured viscosities greater than 1 cP, in the mode of bob (CC27-SN11255) and cup (C-PTD200-SN80218326). The samples were equilibrated to 130 °C±0.1 °C on a thermostatically controlled jacketed assembly to maintain the sample temperature. The samples were cooled to 90 °C±0.1 °C at a rate of 1 °C/min using a circulating water bath. At both temperatures, the samples were stabilized beforehand for 10 min. The rheological behavior of those waxes was evaluated by increasing the shear rate from 1 to 1,000 s^{-1} over a 5 min-time span at both temperatures.

3-2. Water Vapor Transmission Rates (WVTR)

The water vapor transmission rate (WVTR) was measured four times for each operating condition of the forward roll coater using gravimetric cups according to KS T 1305 (Testing method for permeability of damp proof packing material). According to the KS T 1305, upon weighing an assembly containing the samples as the initial weight, the assembly was transferred to a closed chamber containing water (relative humidity 90±2%). The temperature was maintained at 40±1 °C. After 24 h, the assembly was taken out and weighed as the final weight to calculate the water vapor transmission rate.

3-3. Surface Roughness, Coating Weight and Thickness

The surface roughness of wax-coated paper was measured by scanning probe microscopy (Digital Instrument, Nanoscope IIIa) to investigate the fluidity and spreadability of the coated wax on wax-coated paper. The effect of the coupling agent (n-propyl alcohol) on improving the fluidity and the spreadability of the coated wax was also investigated. The width of the web was 0.22 m. The coating weight was measured for each operating condition of the roller speed as well as the clearance of roll millers after the paper was coated and dried for two days under ambient atmospheric conditions. In addition, the thickness of wax-coated paper was determined by Mitutoyo digimatic micrometer from six different parts, and the average was considered to be the thickness of the wax-coated paper.

3-4. Water Resistance

The two types of water-resistant tests were performed on wax-coated paper submerged in water for a set time. One was to measure the dynamic contact angle, of which the advancing angle in particular is used for investigating solid surfaces, between the surface of plate-shaped sample (10 mm×20 mm) of wax-coated paper and the direction of interfacial tension between water phase and air phase by Wilhelmy plate method with dynamic contact analyzer (Cahn, DCA315). The dynamic contact angles of the plate-shaped sample were measured three times (n=3) under each operating condition of the forward roll coater, such as the clearance of two rollers and angular speed of the rollers to show the standard deviation of its measurements in the error bar. The other method was to measure the interfacial tension of the plate-shaped sample between the water phase and air phase with a surface tension meter (Face, CBVP A-3). The original purpose of the surface tension meter was to measure the surface tension of a fixed platinum plate between the designated one among various liquid phases and the air phase.

As the liquid wets the plate, the force F exerted by the meniscus on the plate is measured by a balance or a force transducer consid-

ering weight of the platinum plate and is expressed using the force balance of Eq. (1).

$$F/p=\sigma\cos\theta \quad (1)$$

where p, σ, and θ are the perimeter of the plate, surface tension and contact angle between the outline of the platinum plate surface and the surface of a designated liquid phase, respectively.

The surface tension meter was adapted to the transient water-resistant test in this way. Initially, the bottom line of the plate-shaped sample of wax-coated paper submerged in water for the experimental time, instead of the platinum plate, was positioned at the same level of bulk water. The magnitude of force required to pull up the sample per unit length of the perimeter was equal to that of the component of vapor-liquid interfacial tension (σ) or surface tension in the direction of gravitational force. As the degree of water repellence of wax-coated paper sample decreased under the submerged in water condition, solid-liquid interfacial tension (σ_{SL}) decreased, and it became more wetting. Thus, the contact angle decreased because liquid-vapor (σ) and solid-vapor (σ_{SV}) interfacial tensions were fixed at a constant temperature and pressure. The transient behavior of the contact angle and the force required to pull up the sample per unit length of the perimeter as a component of vapor-liquid interfacial tension (σ) to the direction of gravitational force was observed for 10 h because the degree of water resistance of the sample of wax-coated paper decreased gradually in the water. The surface tension of the plate-shaped samples to the direction of gravitational force (CSTG) was measured three times (n=3) under each operating condition of the forward roll coater, such as the clearance of two rollers and the angular speed of rollers.

3-5. Wet and Dry Tensile Strength

The tensile strength of WJP was measured using a texture analyzer (Stable Micro System, TA-HD 500). The test sample was prepared with a width of 15±0.1 mm and a length of 250 mm according to KS M7014 (Test method of tensile strength for paper and corrugated paper). The wet tensile strength of the submerged test samples was measured in the following way. The test samples were submerged in water for a certain period. The elongation speed was set so that the average time of elongation of the test sample was 20±5 s from the loading time of the texture analyzer until the test sample was broken into pieces. The dry tensile strength of the test samples was also measured under ambient conditions without being submerged in water. The same procedure was repeated to measure the tensile strength of WMP.

3-6. Optical Examination of Wax-coated Fiber Structure

The porous penetration of each wax into the fibrous layer of wax-coated paper was observed with an optical microscope (Olympus, BX60). The coating waxes were three kinds of wax J, wax J with n-propanol, and wax M.

3-7. Antimicrobial Test

The standard fungus of *Aspergillus Terreus* was obtained from KCTC to test the antimicrobial property of the wax-coated papers. The test method of anti-bacteria was in the following manner. The fungus was inoculated in a standard medium composed of starch, sucrose, and agar contained in a petri-dish. Each sample (30 mm× 30 mm) of WJP and WMP was placed in the petri-dish and kept for five days in an incubator maintained at 24 °C. The antimicrobial properties of each wax-coated paper were observed to the degree of crossing over the periphery of the sample. This procedure was repeated after 0.1 g of clinoptilolite powder was added to the surface of each sample of WJP and WMP to test the antimicrobial properties of the clinoptilolite-added wax-coated paper.

RESULTS AND DISCUSSION

1. Rheological Property of Waxes

As rheological property of the waxes, the viscosity of those melt waxes was measured three times (n=3) per experimental condition using a Brookfield viscometer equipped with spindle #3 at an angular speed of 20, 30, 50, 60, and 100 rpm. The correlation between the viscosities and the shear rates applied to those waxes at 90 °C and 130 °C was determined, as shown in Figs. 1(a) and 1(b), respectively. In Fig. 1(a), wax K exhibited power-law fluid behavior between 270 and 500 cP at 90 °C, at which temperature wax K was composed of the melt phase (liquid) and the solid phase (crystalline) due to phase separation. In contrast, the pure liquid phase of wax J exhibited Newtonian fluid behavior around 10 cP at the same temperature. This experimental result is quite consistent with the observations of Ragnarsson et al. [6] and Rosetti

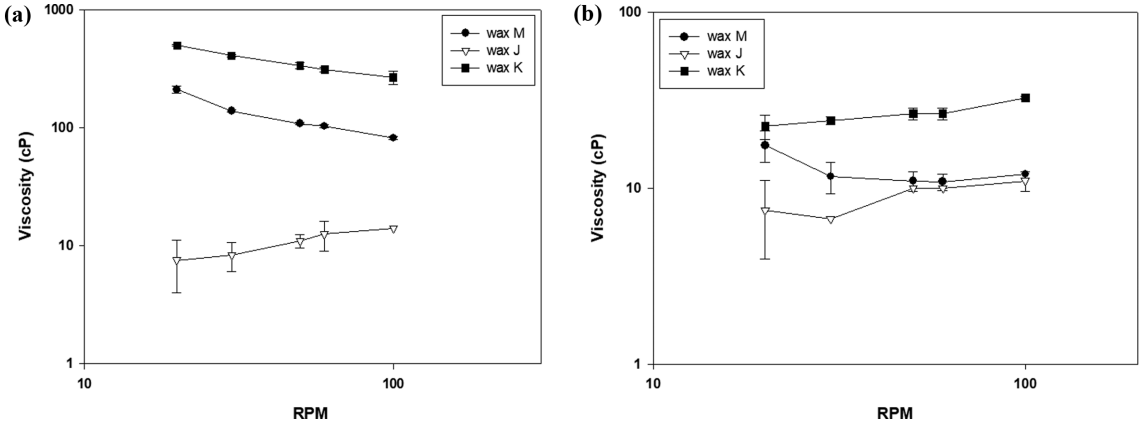

Fig. 1. Rheological property of the waxes at 90 °C and 130 °C (Viscosity versus angular speed of spindle #3 of used Brookfield viscometer): (a) 90 °C; (b) 130 °C.

et al. [7] that, once temperatures reach the melting point of paraffin wax, it becomes a liquid with Newtonian properties. Particularly wax M, a blend of seven parts wax K and three parts wax J, exhibited the intermediate behavior of a power-law fluid at viscosity between 70-220 cP. The rheological behavior of waxes K and M at 90 °C was consistent with that of polyethylene wax filled with bentonite reported by Czarneck-Komorowska et al. [8] or that of liquid paraffin filled with MWCNTs reported by Liu et al. [9]. Accordingly, the solid phase including crystalline showing HMTEPs at 116.88 °C and 115.18 °C, of waxes K and M [12], respectively, corresponded to the bentonite and MWCNTs in the experiments of Czarneck-Komorowska et al. [8] and Liu et al. [9], respectively. Therefore, the solid phases including crystalline of waxes K and M behaved as fillers of bentonite in polyethylene wax or additives of MWCNTs in liquid paraffin from the perspective of rheological behavior. Although the exact cause of shear thinning is not fully understood, it is widely regarded to be the effect of interactions in the fluid at the molecular level [29]. In colloid systems, phase separation during flow leads to shear thinning. Czarneck-Komorowska et al. [8] suggested that aggregated structures containing internal suspension medium at a low shear rate broke down to primary particles as shear rates increased. Then, shear-dependent destruction of the filler structure decreased the amount of suspended liquid trapped by particle structures. Accordingly, the effective volume fraction of the filler which determined the viscosity of the suspension, decreased [30]. In addition, a viscosity equation for concentrated solutions or suspensions was derived by Toda and Furuse [31] as an extension of Einstein's hydrodynamic viscosity theory for dilute dispersion of spherical particles. The derivation of the equation is based on the calculation of dissipation of mechanical energy into heat in the dispersion, subtracting the energy dissipation in the portion of solutes or particles. Unlike a suspension system, in polymer systems such as polymer melts and solutions, shear thinning is caused by the disentanglement of polymer chains during flow. At rest, high molecular weight polymers are entangled and randomly oriented. However, when sheared at a high enough rate, these highly anisotropic polymer chains start to disentangle and align along the direction of shear [32]. This leads to less molecular interaction and a larger amount of free space, contributing to shear thinning [33].

This study shows, for the first time, the non-Newtonian shear thinning behavior of not only wax K but also its blend of wax M in terms of their viscosity affected by shear rates at an operating temperature below their melting temperatures of HMTEPs. This study presented a trial for the first time to regard a group of solid phase of crystalline region connected by amorphous region (SCRAR) of waxes K and M, as shown in Fig. 2, as a suspended solid sphere in terms of extended-Einstein viscosity increasing with higher fraction of solid phase in the suspension. Multi-groups of SCRAR of waxes K and M were possible to behave as the fillers in the suspension of melt paraffin wax or melt polyethylene wax. At 90 °C, the multi-groups of SCRAR of waxes K and M interacted with each other to form aggregates, holding a suspending melt wax of LMTEPs trapped by solid phase structures when they sheared at a low rate. However, shear dependent destruction of the aggregates of the multi-groups of SCRAR of waxes K and M decreased the

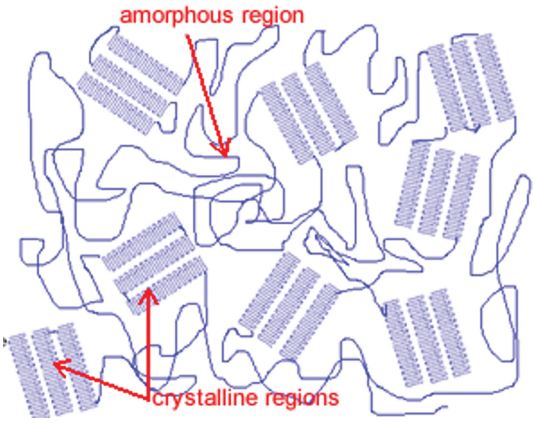

Fig. 2. Schematic diagram of a group of SCRAR of waxes K and M (Adapted from "Crystalline structures in plastics", retrieved from http://www.dynamicscience.com.au/tester/solutions1/chemistry/crystallinestructures.html).

amount of suspended liquid phase of melt paraffin wax or melt polyethylene wax, trapped by solid phase structures. Accordingly, the effective volume fraction of the aggregates, which determined the viscosity of the suspension, decreased. According to the Einstein viscosity equation and its extended equation for concentrated dispersions of solutes [31], the viscosity of a solution increases linearly with the volume fraction of suspended solutes. Nevertheless, the phase separation during flow leads to the behavior of a power law fluid of shear thinning.

In addition, melt paraffin wax or melt polyethylene wax penetrated into the groups of SCRAR of waxes K and M and possibly behaved as a solvent for molecules of amorphous regions of waxes K and M to align with the flow for their orientation to the flow direction. This led to less molecular interaction and a larger amount of free space, again decreasing the viscosity [33]. Therefore, this study shows the non-Newtonian behavior, so-called shear thinning behavior. in the light of characteristics of both suspension systems and polymer systems.

On the other hand, when the temperature was increased to 130 °C, as shown in Figs. 1(b), wax K melted completely so that the viscosity of wax K exhibited Newtonian fluid behavior like wax J. In contrast, the viscosity behavior of wax M was unpredictable because the magnitude of the error bar at 20 rpm was large enough to misinterpret its measured viscosity. Therefore, it was necessary to confirm the experimental results by accurate viscosity measurements using a Physica Rheometer with a guaranteed error range of ±2% for a measured viscosity greater than 1 cP. Accordingly, the viscosity versus shear rate profiles of those waxes were examined using a Physica Rheometer; Figs. 3(a) and 3(b) present their profiles at 90 °C and 130 °C, respectively, where the rheological behavior of those waxes was evaluated by increasing the shear rate from 1 to 1,000 sec^{-1} over a 5 min time span at 90 °C and 130 °C, respectively. In Fig. 3(a), the viscosity profile at 90 °C of these waxes versus the shear rate is almost consistent with the result shown in Figs. 1(a), where 20 and 100 rpm correspond to shear rates of around 20 and 60 s^{-1}, respectively. According to Fig. 3(a), the shear rate of the power-law fluid at 90 °C for wax M was over the entire range

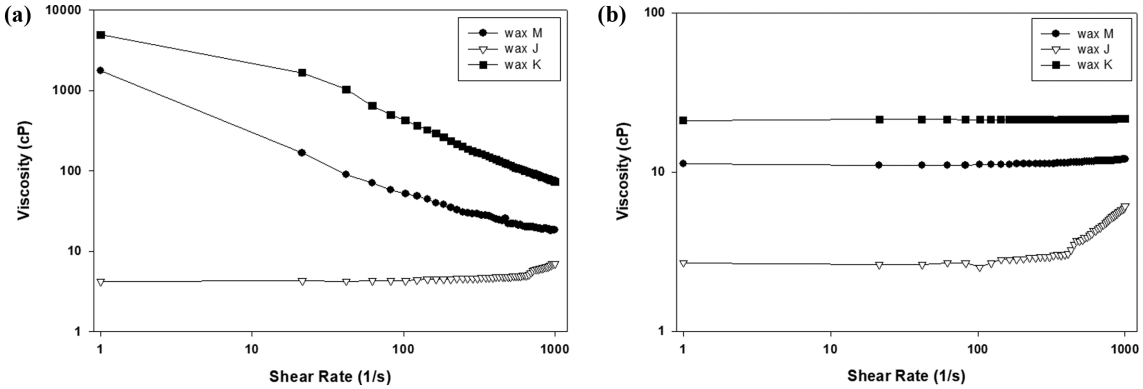

Fig. 3. Rheological property of the waxes at 90 °C and 130 °C (Viscosity versus the shear rate of a Physica Rheometer (ALL ANTON-PAAR INSTRUMENT, MCR 301)): (a) 90 °C; (b) 130 °C.

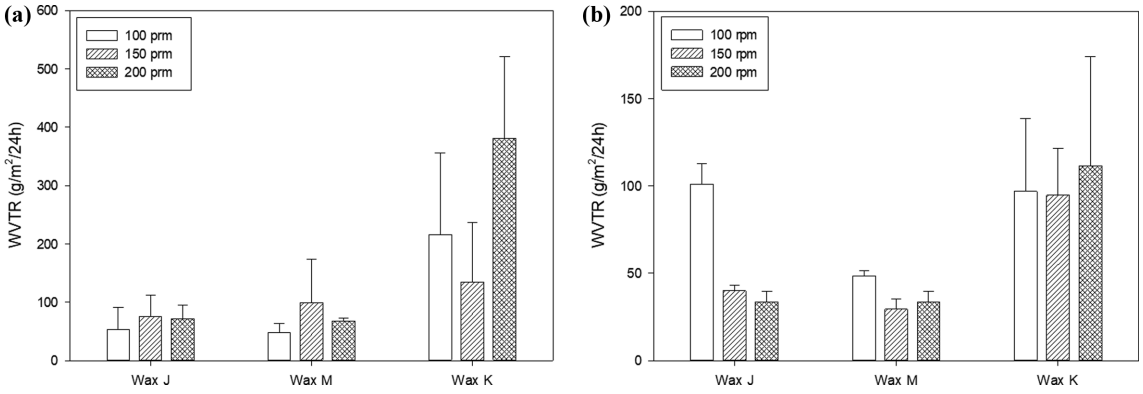

Fig. 4. Water vapor transmission rate (WVTR) of wax-coated papers under the operating condition of roller speed of 100, 150 and 200 rpm, and roller gap of A (WVTR of thin paper (control)=2,546.6±270.4 g/m^2/24 hr): (a) Waxes J, M and K (A=30 μm); (b) waxes J, M and K (A=70 μm).

of shear rates applied in this study, unlike wax K. The viscosity of wax M at a certain shear rate at 90 °C was expected to be equivalent to the one of wax K at ca. twenty-times the shear rate, which belonged to the shear rate-range of a power-law fluid for wax K. Moreover, the viscosity profiles at 130 °C of all the waxes versus shear rate showed Newtonian fluid behavior, as shown in Figs. 3(b), which confirmed the viscosity results for wax K and wax J and clarified the ambiguity for the viscosity behavior of wax M shown in Figs. 1(b). Wax J also showed the behavior of dilatant fluid because the viscosity of wax J increased continuously with increasing shear rate above the range of 404 s^{-1} at 130 °C, as shown in Fig. 3(b).

The two melting points of waxes J, K, and M were reported to be 47.53/64.10 °C, 73.16/116.88 °C, and 59.03/115.18 °C, respectively, according to the previous investigation by Lee et al. [12]. As the operating temperature of feed (waxes) bath of the forward roll coater in this study was maintained at 120 °C, each fed wax remained as a melt state, with a negligible amount of crystalline-phased wax, particularly for waxes M and K. In addition to wax J, waxes M and K would behave as Newtonian fluids in the forward roll coater operation of this study, and would show a viscosity slightly higher than 12 and 21 cP, as shown in Fig. 3(b), in the forward roll coater operation of this study, respectively. These viscosities were consistent with a typical forward roll coating parameter of 1-50 mPa s viscosity liquids [28].

2. Water Vapor Transmission Rates (WVTR)

The water vapor transmission rates (WVTR) generally increase in the order of WMP, WJP, and WKP, according to Fig. 4. The WVTR of wax WJP in this study was ca. ten-times as high as that of paraffin wax reported by Bucio et al. [4], considering that the thickness of paraffin wax-samples for their WVTR experiments was ca. 7-17 times as thick as the roller-gap of the forward roll coater in this study. Moreover, the WVTR of WJP in this study was close to that of beeswax investigated by Mishra et al. [5], which was equivalent to the upper bound of the WVTR of WJP in this study. According to Fig. 4, the effects of wax M on the barrier properties were equivalent to or even superior to that of wax J. The minimum WVTR of 29.4(±5.9) g/m^2/day was achieved using WMP under the coating condition of experiment II (70 μm of roller gap) and 150 rpm, as shown in Fig. 4. WMP even exhibited better barrier properties than the latex dispersion coating based on styrene-butadiene (SB) polymers in the investigation by Schuman et al. [17]. Therefore, in this study, WMP had a lower WVTR than WJP, and has been suggested as a replacement for wax J as a coating agent to a thin paper.

3. Surface Roughness and Coating Weight

The fluidity and the spreadability of coated wax on wax-coated

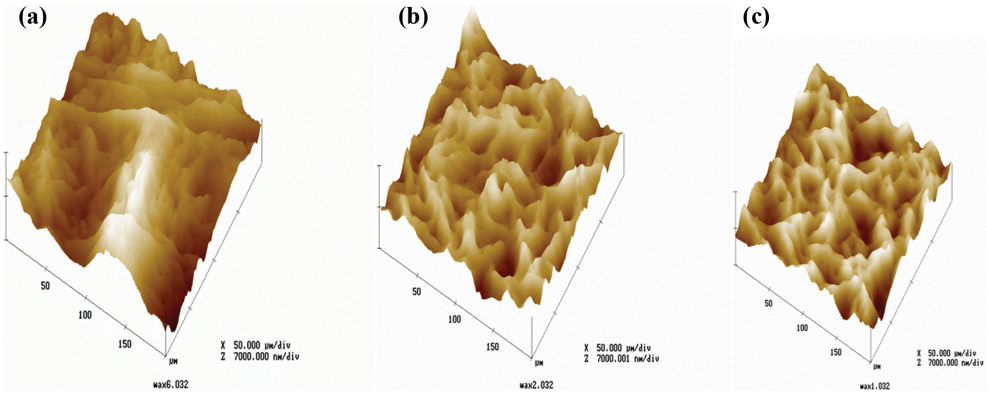

Fig. 5-1. Surface mean roughness of WJP under the operating condition of roller gap of 30 μm and various angular velocity: (a) 1.347 μm (100 rpm); (b) 850.91 nm (150 rpm); (c) 815.87 nm (200 rpm).

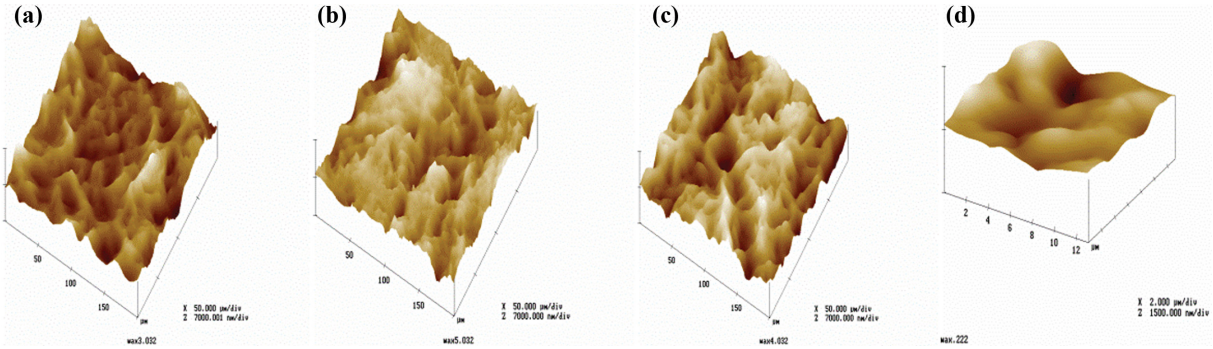

Fig. 5-2. Surface mean roughness of WJP under the operating condition of roller gap of 70 μm and various angular velocity: (a) 705.09 nm (100 rpm); (b) 781.49 nm (150 rpm); (c) 917.44 nm (200 rpm); (d) 119.43 nm (150 rpm, n-propanol-added WJP).

paper surface correlated with such operating conditions of two-roll forward roll coater as two rolls' rpm and gap. In Figs. 5-1(a), 1(b), and 1(c), the three-dimensional images of the WJP surface are shown, respectively, with the operating condition of 100 rpm, 150 rpm, and 200 rpm for the experiment I (i.e., 30 μm gap of rolls of the forward roll coater). Figs. 5-1(a), 1(b), and 1(c) present the corresponding mean surface roughness of 1.347 μm, 850.91 nm, and 815.87 nm for the WJP surface, respectively. Their mean surface roughness decreased with increasing rpm of the rolls for the experiment I. In Figs. 5-2(a), 2(b), and 2(c), the 3-dimensional images of the wax J-coated surface are shown, respectively, with the operating condition of 100 rpm, 150 rpm, and 200 rpm for experiment II (i.e., 70 μm gap of rolls of the forward roll coater). Figs. 5-2(a), 2(b), and 2(c) show the corresponding mean surface roughness of 705.09 nm, 781.49 nm, and 917.44 nm for the WJP surface, respectively. In contrast to the case of 30 μm rolls-gap of the forward roll coater, their mean surface roughness increased with increasing rpm of rolls in a 70 μm roll-gap of the forward roll coater. On the other hand, from the point of view of the order of magnitude analysis, the results of the mean waxed surface roughness were on the order of ca. 800 nm regardless of the operating conditions, such as roller speed and rollers gap of a two-roll forward roll coater. The effect of the coupling agent (n-propyl alcohol) on improving the fluidity and the spreadability of the coated wax was also investigated. When n-propanol was added as a coupling agent for the operating condition of 150 rpm and 70 μm gap of rolls of the forward roll coater, the surface mean roughness was 119.43 nm, as shown in Fig. 5-2(d), which showed much smoother conditions than 781.49 nm of the case (with the same operating condition) without n-propanol, as shown in Fig. 5-2(b). In particular, the surface mean roughness of 119.43 nm as shown in Fig. 5-2(d), in this study was even smoother than the optimized ones in wax mix at three levels of used paraffin wax reported by Katiyara et al. [14].

Thus, the fluidity and the spreadability of wax J were improved greatly by the addition of n-propanol. The surface roughness of WJP, WMP, and WKP were compared in terms of the roller speed and the roller gap, as shown in Fig. 5-3. The surface roughness of waxes for any coating condition increased in the order of WMP, WKP, and WJP according to Fig. 5-3. Therefore, the surface roughness and barrier property of WVTR were minimized and enhanced, respectively, by blending waxes J and K. From a comprehensive point of view, the reasons can be explained, as follows, why 1) WVTR increased in the order of waxes M, J, and K; 2) the surface roughness of waxes increased in the order of waxes M, K, and J. First, regarding WVTR, unfractionated wax K contains more hydrophilic functional groups than wax J. Accordingly, WVTR of WJP turned out to be less than the one of WKP. Moreover, according to Lee et al. [34], lowering surface roughness of thin layer was very effective to decrease WVTR. The reason why WVTR of WMP was less than the one of WJP was suggested that the sur-

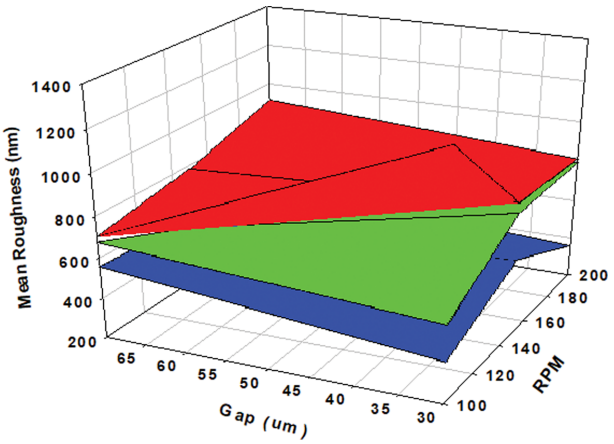

Fig. 5-3. Surface mean roughness of WJP (red), WMP (blue), and WKP (green) under the operating condition of roller speed of 100, 150 and 200 rpm, and roller gap of 30 and 70 μm.

face roughness of wax-coated papers for any coating condition increased in the order of WMP, WKP, and WJP in this study. Secondly, regarding the surface roughness, the reasons were suggested that 1) hydrophilic and hygroscopic cellulose of paper interacted with waxes, and was penetrated deeper and wider into its pores by wax M and wax K than wax J, as shown in the latter part of this study, because unfractionated wax K contains more hydrophilic functional groups than wax J; 2) According to Lee et al. [12], wax M, a blend of wax K and wax J, still had the thermal properties of HMTEP at the melting temperature of 115.18 °C, which were even narrower and lower than those of wax K, respectively. Therefore, wax M was suggested to have better thermal property to be coated for wax-coated papers than wax K, under the coating conditions of this study.

Accordingly, the remaining properties of the WJP and WMP, including their water resistance, were characterized and compared in the latter part of this study.

Fig. 5-4 shows the coating weights of WJP, WMP, and WKP under each operating condition of the roller speed and roller gap. In the forward roll coating, the coating thickness was sensitive to the speed, viscosity, and gap [28]. Fig. 5-4 shows that the coating weight was dependent on the operating conditions of the forward roll coater, such as the roller speed and roller gap. Among the operating parameters, the roller gap was the major parameter, and the roller speed was the minor parameter as far as the coating weight was concerned. The coating weight decreased with decreasing roller gap. When the roller gap was as narrow as 30 μm of experiment I, the coating weight decreased with increasing rpm of the rollers. It corresponded to the experimental result that the mean surface roughness of WJP decreased with increasing rpm of the rolls for the experiment I. When the roller gap was as wide as 70 μm of experiment II, the coating weight was not heavily depen-

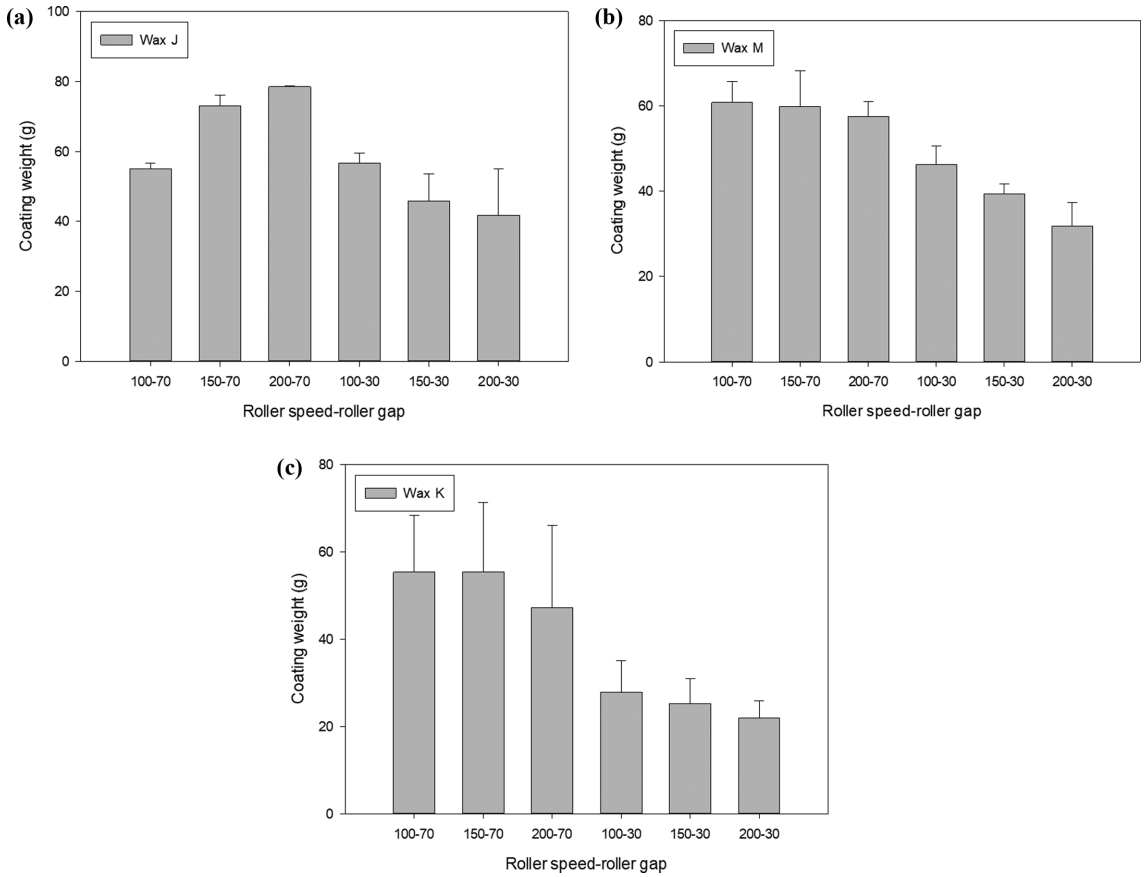

Fig. 5-4. Coat weights of waxes J, M, and K for each operating condition of roller speed (rpm) and clearance (μm) of roll millers (roller speed-clearance): (a) Wax J; (b) wax M; (c) wax K.

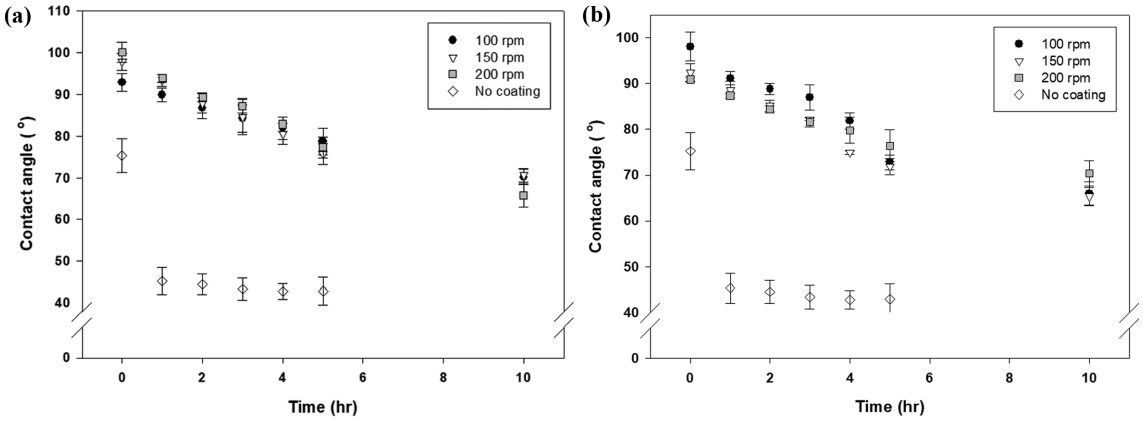

Fig. 6. Advancing dynamic contact angles of WJP submerged in water under the operating condition of roller speed of 100, 150 and 200 rpm: (a) Roller gap of 30 μm; (b) roller gap of 70 μm.

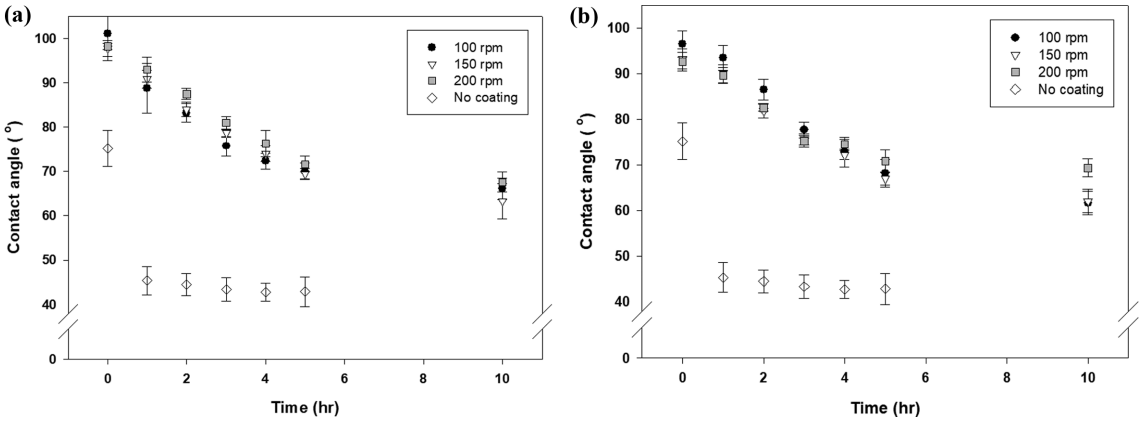

Fig. 7. Advancing dynamic contact angles of WMP submerged in water under the operating condition of roller speed of 100, 150 and 200 rpm: (a) Roller gap of 30 μm; (b) roller gap of 70 μm.

dent on the roller speed except for WJP, in which the coating weight increased with increasing roller speed. It also corresponded to the experimental result that in contrast to the case of 30 μm rolls-gap of the forward roll coater, the mean surface roughness of WJP increased with increasing rpm of rolls in a 70 μm roll-gap of the forward roll coater.

4. Water Resistance

Figs. 6(a)-(b), and Figs. 7(a)-(b) show the degree of water resistance as the transient magnitude of dynamic contact angles for WJP and WMP, respectively, while the wax-coated samples were submerged in water for each designated time. Figs. 6(a) and Fig. 7(a) present the behavior of dynamic contact angles for the three operating conditions (100, 150, and 200 rpm) of the forward roll coater when the clearance of two rolls of the forward roll coater was set to 30 μm (experiment I). Similarly, Fig. 6(b) and Fig. 7(b) present the case when the clearance of two rolls of forward roll coater was set at 70 μm (experiment II). The dynamic contact angle of a coated sample decreased with increasing submerged time of the coated sample, suggesting that the coated samples gradually lost their hydrophobicity as hydrophilic functional groups of the coated wax moved forward to the interface between water and coated wax under water-submerged condition [13]. Up to 10 h of water submerged condition applied to WJP and WMP, the magnitude of the dynamic contact angle for the fastest roller speed of 200 rpm was generally larger or ultimately larger than that for the slowest roller speed of 100 rpm. The behavior of dynamic contact angles of experiment I of wax M, as shown in Fig. 7(a), was generally consistent with that of experiment I of wax J for the three operating conditions (100, 150, and 200 rpm) of the forward roll coater, as shown in Fig. 6(a), when the clearance of two rolls of the forward roll coater was set to 30 μm. The behavior of the dynamic contact angles of experiment II of wax M, as shown in Fig. 7(b), was also similar to that of experiment II of wax J under the three operating conditions (100, 150, and 200 rpm) of the forward roll coater, as shown in Fig. 6(b), when the clearance of two rolls of the forward roll coater was set to 70 μm. Regardless of both the clearance and angular speed of two rollers, the magnitude of dynamic contact angles for WJP and WMP generally decreased continuously from 90-100° (initial dry condition) to 65-75° at 10 h of the experiment. At 5 h, however, the dynamic contact angle of WJP was generally ca. 10° higher than that of WMP, indicating that the degree of water repellence of WJP was slightly greater than that of WMP. Nevertheless, the difference in the dynamic contact angles was insignificant at 10 h.

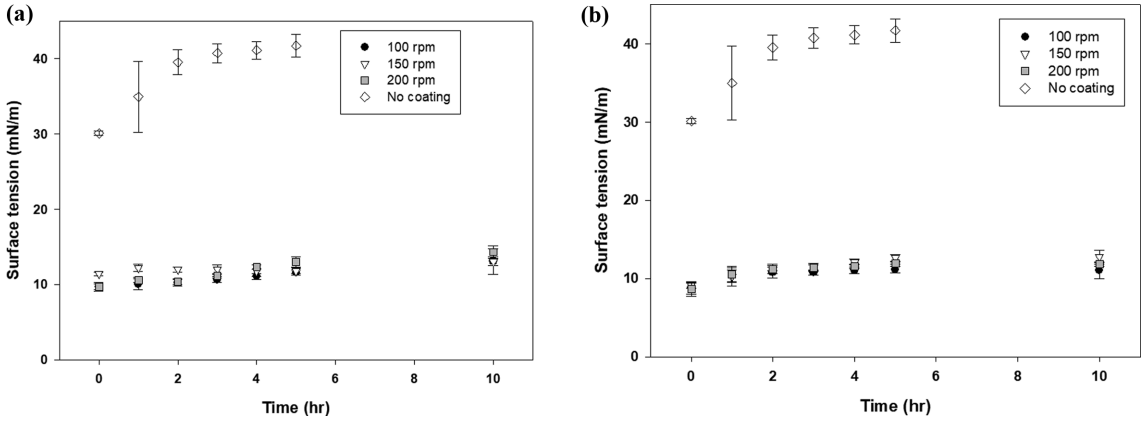

Fig. 8. CSTG of WJP submerged in water under the operating condition of roller speed of 100, 150 and 200 rpm: (a) Roller gap of 30 μm; (b) roller gap of 70 μm.

Figs. 8(a) and 8(b) show the transient behavior of the components of surface tension to the direction of gravitational force (CSTG) for experiment I and II of WJP, respectively. The dried sample was ca. 11 mN/m and 9 mN/m for experiments I and II, respectively, and the saturated values for experiments I and II, were ca. 13 mN/m and the one slightly below 13 mN/m, respectively. For both experiments I and II, their values were affected insignificantly by the angular speed of rollers such as 100, 150, and 200 rpm. Fig. 9 shows the transient behavior of CSTG when n-propanol (10, 20, and 30 cc) was added to wax J as a coupling agent. Their saturated values increased dramatically up to ca. 35 mN/m at 10 h of the water-submerging period. Regardless of the amount of n-propanol, their transient and saturated values were similar. Figs. 10(a) and 10(b) show the transient behavior of CSTG for experiment I and II of WMP, respectively. The values of the dried sample of WMP were ca. 10 mN/m for experiments I and II, which was similar to those of WJP for experiments I and II. On the other hand, their saturated values ranged between 30 and 35 mN/m, which were two- to three-times greater than those for WJP. They were similar to those for n-propanol added WJP. According to Eq. (1), the static contact angle (θ) may be inversely estimated by the arc cosine value of its measured value of CSTG divided by σ of water (i.e., 72.8 mN/m [16]).

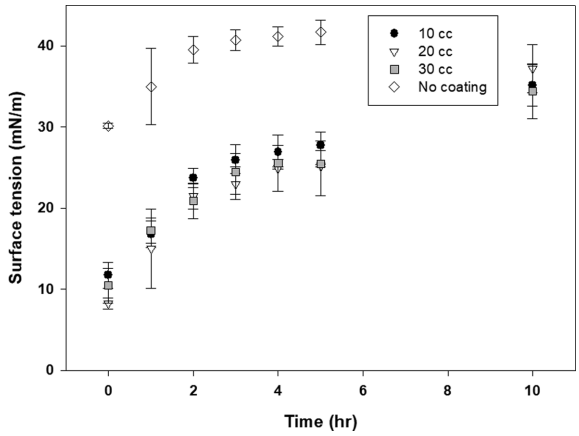

Fig. 9. CSTG of various amounts of n-propanol-added (10, 20 and 30 cc) WJP submerged in water under the operating condition of roller speed of 150 rpm and roller gap of 30 μm.

Under dry condition, CSTG for both WMP and WJP was the same as ca. 10 mN/m, which corresponded to the estimated static contact angle of 82° while the magnitude of dynamic contact

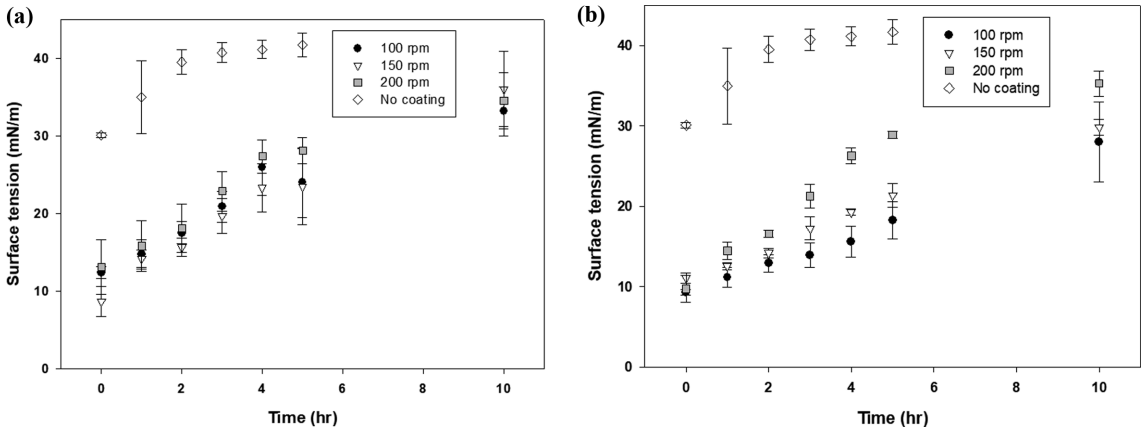

Fig. 10. CSTG of WMP submerged in water under the operating condition of 100, 150 and 200 rpm: (a) Roller gap of 30 μm; (b) roller gap of 70 μm.

angles for WMP and WJP were distributed at the range of 90-100° at the initial dry condition as shown in Figs. 6 and 7. For WMP and WJP, using the saturated values under water-submerged condition of 10 h, of 35 mN/m and 13 mN/m, the static contact angles were estimated to be 61° and 80°, respectively. The estimated static contact angle of WJP under water submerged condition evolved from 82° at initial dry condition to 80° at the saturated condition (water-submerged condition of 10 h), while Garai et al. [15] reported that the measured static contact angles evolved from initial 85° to 72° for 35 s at water-paraffin wax treated wood substrate interface.

For WMP and WJP, the estimated static contact angles of 61° and 80° at the saturated values, respectively, were close to the dynamic (advancing) contact angle, which gives the maximum value that the static contact angle can have on the surface, of 65-75° at 10 h of the experiment, as shown in Figs. 6 and 7. Therefore, in the case of WMP, the results of CSTG were consistent with those of dynamic contact angle in terms of the water resistance. In the case of WJP, however, both results led to the contradiction that the estimated static contact angle of 80° exceeded its range of dynamic contact angle by at least 5°, in terms of water resistance, resulting from a possible fibrous structural uncertainty of WJP and instability of wax J, which penetrated the fibrous structure of WJP, against water resistance. The possible fibrous structural uncertainty of WJP and instability of wax J adversely affected the hydrophobicity of the wax-coated surface. For experiments I, CSTG values for WMP were relatively unaffected by the angular speed of rollers (100, 150, and 200 rpm) like those for WJP and n-propanol-added WJP. For experiment II, however, CSTG values for WMP were affected by the angular speed of the rollers (100, 150, and 200 rpm), unlike the other cases, even though the lowest degree of water repellence at 200 rpm from experiment II of WMP was generally similar to the degree of water repellence from experiment I of WMP.

5. Wet and Dry Tensile Strength

The tensile strength of the wax-coated samples decreased with increasing submerged time in water. Figs. 11(a) and 11(b) show the time-dependent behavior of tensile strength of the WJP sample, where its values of dry condition for experiments I and II were ca. 2 kg_f and decreased to a saturated value of ca. 1.5 kg_f (i.e., 75% of initial tensile strength) when the test samples were submerged in water for 10 h. Figs. 12(a) and 12(b) present the time-dependent behavior of tensile strength of the WMP sample. Their values of the dry condition for experiments I and II were the same as or higher than those of the WJP samples, which, however, decreased to a saturated value of ca. 1 kg_f (i.e., ca. 50% of initial ten-

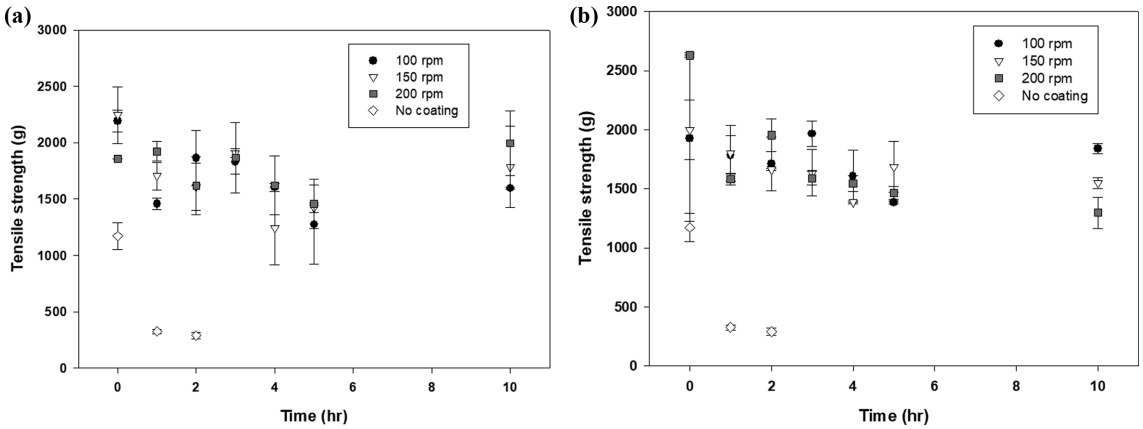

Fig. 11. Tensile strength of WJP submerged in water under the operating condition of 100, 150 and 200 rpm: (a) Roller gap of 30 μm; (b) roller gap of 70 μm.

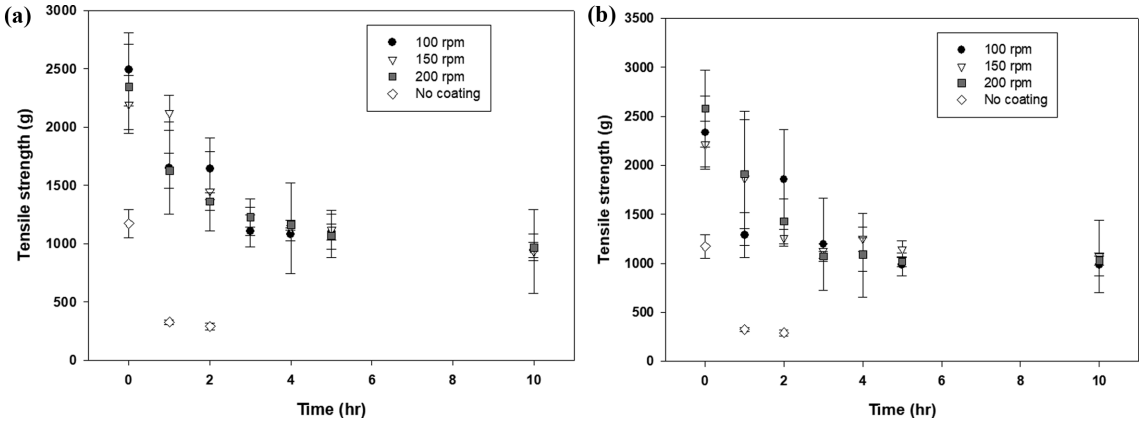

Fig. 12. Tensile strength of WMP submerged in water under the operating condition of 100, 150 and 200 rpm: (a) Roller gap of 30 μm; (b) roller gap of 70 μm.

sile strength) when the WMP samples were submerged in water for 10 h. Therefore, the tensile strength of the WMP sample was ca. 0.5 kg_f lower than that of the WJP sample for 10 h-wet conditions.

According to Lee et al. [13], the blend of wax M behaved unlike wax K but similarly to wax J in terms of the change in hydrophobicity. The diffusivity values of the hydrophilic functional groups of waxes were established under one-day water-submerged conditions, 1.35×10^{-11} cm^2/s and 1.96×10^{-11} cm^2/s for waxes J and M, respectively. This is because the diffusivity can be estimated in such a criterion that $D\sim(l^2/t)$, where l and t are the traveling distance and time, respectively. Therefore, the ratio of traveling distances of hydrophilic functional groups between waxes M and J can be expressed as $\sqrt{D_M/D_J}\sim1.2$, where D_M and D_J represent the diffusivity of waxes M and J. Upon wax-coating on a thin paper, the hydrophilic functional groups of the coated wax would migrate into a fibrous structure of the thin paper. Assuming the thin paper was coated with the same amount of waxes, the portion of coated wax M penetrating its fibrous structure would be more by 20% than that of wax J, which led to a thinner coating of wax M than wax J above the surface of the thin paper. According to Fig. 13, thicknesses of WJP and WMP were close to each other regardless of roller speeds in the case of roller gap of 30 μm. However, in the case of roller gap of 70 μm, thickness of WJP was generally thicker by ca. 45 μm than those of WMP.

In a biological system, a hydrophobic component of the source could be transferred successfully to a hydrophobic sink via a hydrophilic medium and vice versa [35]. Therefore, it was suggested that

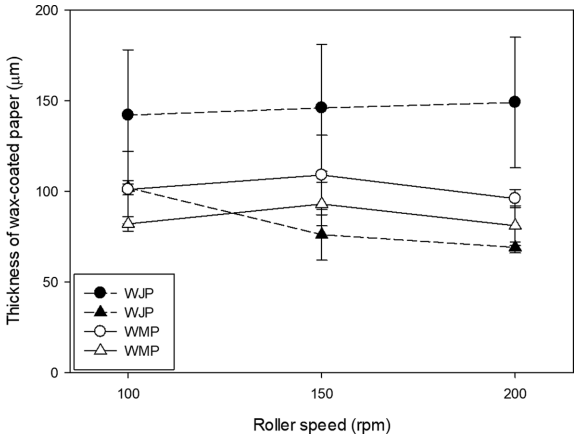

Fig. 13. Thickness of WJPs (●, roller gap of 70 μm; ▲, roller gap of 30 μm) and WMP (○, roller gap of 70 μm; △, roller gap of 30 μm).

even if the hydrophobicity on the surface and in the body above the thin paper of the coated waxes remains intact, water molecules may be transferred to the hydrophilic fibrous structure of the thin paper through the coated waxes as a medium during the water-submerged condition. Under the circumstances, more water molecules can be transferred via the wax M than the wax J coating because the coating thickness of WMP, above the surface of the thin paper, would be thinner than that of WJP. The WMP hold-

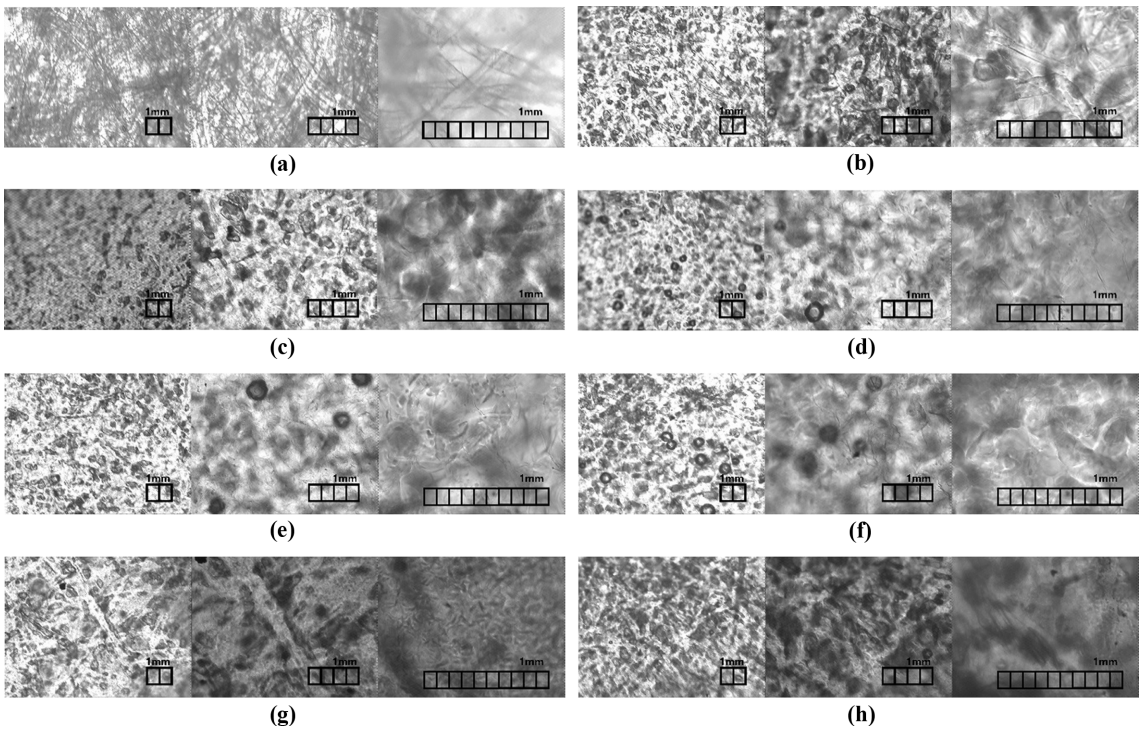

Fig. 14. Optical examination (x30, x60, x150) of bare or wax-coated fiber structure coated under the operating condition of roller gap of A and roller speed of 200 rpm: (a) Bare-thin paper; (b) WJP (A=30 μm); (c) WJP (A=70 μm); (d) n-propanol 10 mL-added WJP (A=30 μm); (e) n-propanol 20 mL-added WJP (A=30 μm); (f) n-propanol 30 mL-added WJP (A=30 μm); (g) WMP (A=30 μm); (h) WMP (A=70 μm).

ing more water molecules in its fibrous structure of the thin paper would be imparted with the less tensile strength, as shown in Figs. 11 and 12, and it would have inversely affected the hydrophobicity of wax-coated surface facing water-phase to be reduced more drastically upon saturation than the WJP.

6. Optical Examination of Wax-coated Fiber Structure

Fig. 14 presents the patterns of porous penetration into the fibrous structure of the thin paper coated with none (a), WJP (b), (c), n-propanol-added (10, 20, and 30 mL) WJP (d)-(f), and WMP (g), (h), respectively. As shown in Figs. 14(b) and 14(c), the family of many small wax J-clots penetrated the fibrous pores of the thin paper for experiments I and II, respectively. On the other hand, for n-propanol-added WJP, the more n-propanol was added, wider formed clots were spread into the fibrous pore structure of the thin paper, as shown in Figs. 14(d) to 14(f), suggesting that the property of the fibrous pore structure of the thin paper was rather hydrophilic. Interestingly, the formed clots of WMP were spread smoothly into the fibrous pore structure of the thin paper like n-propanol-added WJP, as shown in Figs. 14(g) and 14(h). This was consistent to that the coating heights above the surface of the thin paper, of WJP were estimated to be thicker than those of WMP. Thus, the capillary pressure forces for WMP and n-propanol-added WJP were observed greater than that for WJP.

The deeper and wider porous penetration of WMP was also suggested to contribute to the improved heat-stability of the wax-coated paper owing to the melting temperature of HMTEP for wax M, higher than the one for wax J.

7. Antimicrobial Test

Lately, the application of a specific natural zeolite material, clinoptilolite, has been documented in human and veterinary medicine. Many recognized positive medical effects of clinoptilolite have been attributed to its basic material properties, particularly to its reversible ion-exchange and adsorption capacity [36]. In particular, cation exchange is one of the properties of zeolites that gives them prolonged antimicrobial properties. This makes zeolites microbicide properties of great interest not only in food pathogen application, but over a wide range of applications against Gram-positive and Gram-negative bacteria [37]. Accordingly, clinoptilolite has been tested as a possible supplementation to broilers feed as an alternative to antibiotics [38]. Figs. 15(a) to 15(d) present the antimicrobial properties of WJP, clinoptilolite-added WJP, WMP, and clinoptilolite-added WMP, respectively. For the WJP, many colonies of *Aspergillus Terreus* were observed on its periphery and its surface, as shown in Fig. 15(a). On the other hand, as shown in Fig. 15(c), there were obvious constructed lines against microbial growth found on the periphery of the sample of the WMP. Thus, the antimicrobial property of the wax M-coated sample was superior to that of the wax J-coated sample. In addition, Figs. 15(b) and 15(d) show the excellent antimicrobial properties of clinoptilolite added to wax J and wax M, respectively.

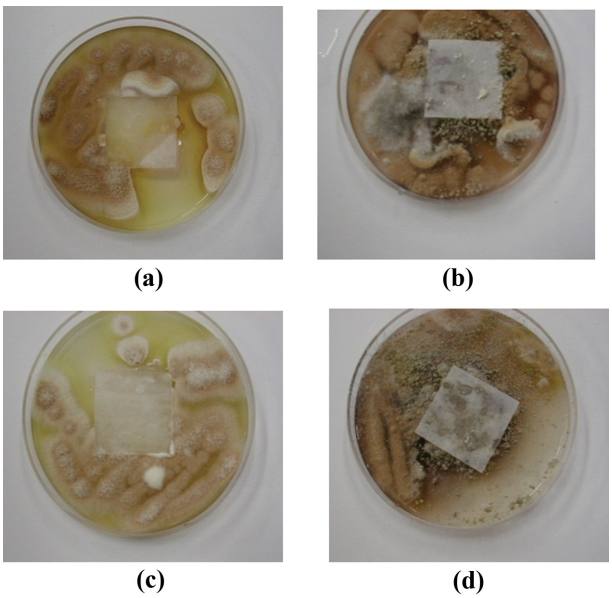

Fig. 15. Anti-microbial property against the standard fungus of *Aspergillus Terreus*: (a) WJP; (b) clinoptilolite powder-topping WJP; (c) WMP; (d) clinoptilolite powder-topping WMP.

CONCLUSIONS

This paper, for the first time, presented non-Newtonian shear thinning behavior of not only wax K but also its blend of wax M in terms of their viscosity affected by shear rate at an operating temperature below their melting temperature of HMTEPs. They showed the non-Newtonian behavior, so-called shear thinning behavior, at 90 °C in the light of characteristics of both suspension systems and polymer systems. In addition, the profiles of viscosity at 130 °C of all the waxes versus the shear rate exhibited Newtonian fluid behavior. Wax J also showed the behavior of a dilatant fluid because the viscosity of wax J increased continuously with increasing shear rate above the range of 404 s^{-1} at 130 °C. The water vapor transmission rate (WVTR) generally increased in the order of WMP, WJP, and WKP. The minimum WVTR of 29.4(±5.9) g/m^2/day was achieved using WMP under the coating condition of experiment II (70 μm of roller gap) and 150 rpm. Thus, the effects of wax M on the barrier properties were equivalent to or even superior to those of wax J. The surface roughness of waxes for any coating condition increased in the order of WMP, WKP, and WJP. Accordingly, the surface roughness and the barrier property of WVTR were minimized and enhanced, respectively, by blending waxes J and K. Therefore, in this study, wax M was suggested to replace wax J as a coating agent on thin paper.

The measured dynamic contact angles indicated that both WJP and WMP showed similar hydrophobicity or water-resistant property, even though the results of CSTG, which may be converted to the static contact angle, indicated that both WMP and n-propanol-added WJP showed similar water-resistance or hydrophobicity, which was weaker than the one for the WJP. In the case of WMP, the results of CSTG were consistent with those of dynamic contact angle in terms of the water resistance. However, in the case of WJP, both results led to a contradiction in terms of water resistance, resulting from a possible fibrous structural uncertainty of WJP and instability of wax J penetrating the fibrous structure of WJP against water resistance. Those experimental results of CSTG of the WMP were consistent with its saturated tensile strength, which

was less by 33% than the one of WJP.

As a result of optical examination of wax-coated fiber structure, the formed clots of WMP were spread smoothly into the fibrous pore structure of the thin paper like n-propanol-added WJP. This was consistent to that the coating heights above the surface of the thin paper, of WJP were estimated to be thicker than those of WMP. Nevertheless, a deeper and wider porous penetration of wax M was also suggested to contribute to the improved heat-stability of WMP owing to the melting temperature of HMTEP for wax M, higher than the one for wax J. In addition, the antimicrobial property of the WMP sample was superior to the WJP sample. Nevertheless, the antimicrobial property of the WJP sample was enhanced remarkably by the addition of clinoptilolite.

REFERENCES

1. L. Ren, L. Men, Z. Zhang, F. Guan, J. Tian, B. Wang, J. Wang, Y. Zhang and W. Zhang, *Int. J. Environ. Res. Public Health*, **16**, 1941 (2019).
2. J. Yang, Y. Yang, W. M. Wu, J. Zhao and L. Jiang, *Environ. Sci. Technol.*, **48**, 13776 (2014).
3. F. Kawai, M. Watanabe, M. Shibata, S. Yokoyama, Y. Sudate and S. Hayashi, *Polym. Degrad. Stab.*, **86**, 105 (2004).
4. A. Bucio, R. Moreno-Tovar, L. Bucio, J. Espinosa-Davila and F. Anguebes-Franceschi, *Coatings*, **11**, 261 (2021).
5. B. Mishra, B. S. Khatkar, M. K. Garg and L. A. Wilson, *J. Food Sci. Technol.*, **47**(1), 109 (2010).
6. R. Ragnarsson, J. L. Ford, C. D. Santangelo and E. Bodenshatz, *Phys. Rev. Lett.*, **76**, 3456 (1996).
7. F. Rossetti, G. Ranalli and C. Faccenna, *J. Struct. Geol.*, **21**, 413 (1999).
8. D. Czarneck-Komorowska, K. Grzeskowiak, P. Popielarski, M. Barczewski, K. Gawdzinska and M. Poplawski, *Materials*, **13**, 2255 (2020).
9. X. Liu, H. I. Mohammed, A. Z. Ashkezari, A. Shahsavar, A. K. Hussein and S. Rostami, *J. Mol. Liq.*, **300**, 112269 (2020).
10. A. P. Dwivedi, G. K. Ghosal and P. N. Belkhode, *International J. of Research in Science and Engineering*, CHEMCON special issue, 192 (2018).
11. W. Ciesinska, B. Liszynska and J. Zielinski, *J. Therm. Anal. Calorim.*, **125**, 1439 (2016).
12. E. J. Lee, J. K. Park, Y.-S. Lee and K.-H. Lim, *Korean J. Chem. Eng.*, **27**(2), 524 (2010).
13. E. J. Lee, Y.-S. Lee and K.-H. Lim, *Korean J. Chem. Eng.*, **27**(2), 518 (2010).
14. J. K. Katiyara, N. Yadav, N. Singh and V. K. Pal, *Appl. Mech. Mater.*, **110-116**, 627 (2012).
15. R. M. Garai, I. C. Sanchez, R. T. Garcıa, M. A. R. Valverde, M. A. C. Vilchez and R. Hidalgo-Alvarez, *J. Dispers. Sci. Technol.*, **26**, 9 (2005).
16. N. M. Salih, U. Hashim, N. Nafarizal, C. F. Soon and M, Sahdan, *Adv. Mater. Res.*, **832**, 773 (2014).
17. T. Schuman, B. Adolfsson, M. Wikstrom and M. Rigdahl, *Prog. Org. Coat.*, **54**, 188 (2005).
18. T. Schuman, A. Karlsson, J. Larsson, M. Wikstrom and M. Rigdahl, *Prog. Org. Coat.*, **54**, 360 (2005).
19. T. Schuman, M. Wikstrom and M. Rigdahl, *Prog. Org. Coat.*, **51**, 228 (2004).
20. Y. Pan, H. Xiao and Z. Song, *Cellulose*, **20**, 485 (2013).
21. Z. Song, H. Xiao and Y. Zhao, *Carbohydr. Polym.*, **111**, 442 (2014).
22. Y. Pan, F. Wang, T. Wei, C. Zhang and H. Xiao, *Chem. Eng. J.*, **302**, 33 (2016).
23. F. Guan, Z. Song, F. Xin, H. Wang, D. Yu, G. Li and W. Liu, *J. Bioresour. Bioprod.*, **5**, 39 (2020).
24. V. S. Saji, *Colloids Surf. A*, **602**, 125132 (2020).
25. D. W. Wei, H. Wei, A. C. Gauthier, J. Song, Y. Jin and H. Xiao, *J. Bioresour. Bioprod.*, **5**, 1 (2020).
26. H. Teisala, M. Tuominen and J. Kuusipalo, *Adv. Mater. Interfaces*, **1**, 1300026 (2014).
27. I. Yakimets, N. Wellner, A. C. Smith, R. H. Wilson, I. Farhat and J. Mitchell, *Polymer*, **46**, 12577 (2005).
28. D. J. Coyle, in *Liquid film coating*, S. F. Kistler and P. M. Schweizer Eds., Chapman & Hall, London, U. K. (1997).
29. R. Datta, L. Yelash, F. Schmid, F. Kummer, M. Oberlack, M. Lukacova-Medvidova and P. Virnau, arXiv:2101.03645 [cond-mat.soft] (2021).
30. S. Kuzbeck, J. Kaschta and H. Munstedt, *Rheol. Acta*, **35**, 446 (1996).
31. K. Toda and H. Furuse, *J. Biosci. Bioeng.*, **102**(6), 524 (2006).
32. G. Trotta, B. Stampone, I. Fassi and L. Tricarico, *Polym. Testing*, **96**, 107068 (2021).
33. R. Datta, L. Yelash, F. Schmid, F. Kummer, M. Oberlack, M. Lucacova-Medvidova and P. Virnau, *Polymers*, **13**, 2806 (2021).
34. S.-Y. Lee, B.-W. Shin and H.-R. Lee, *Mol. Cryst. Liq. Cryst.*, **586**(1), 123 (2013).
35. H. H. Wang, G. Garruti, M. Liu, P. Portincasa and D. Q.-H. Wang, *Ann. Hepatol.*, **16**(Suppl. 1), s27 (2017).
36. C. Cerbu, V. A. Ilas, M. Czopowicz, A. V. Potarniche, E.-P. Bodart-Nieva, E. A. Muresan, J. Kaba, M. Spinu and E. Pall, *Animals*, **10**(12), 2284 (2020).
37. F. Ozogul, V. Simat, S. Gokdogan, J. M. Regenstein and Y. Ozogul, *Front. Microbiol.*, **9**, 2585 (2018).
38. S. K. Pavelic, J. S. Medica, D. Gumbarevic, A. Filosevic, N. Przulj and K. Pavelic, *Front. Pharmacol.*, **9**, 1350 (2018).